BNL-113649-2017-JA

All The Catalytic Active Sites of MoS2 for Hydrogen Evolution

Guoqing Li, Du Zhang, Qiao Qiao, Yifei Yu, David Peterson, Raj Kumar, Stefano Curtarolo, Frank Hunte, Steve Shannon, Yimei Zhu, Weitao Yang, and Linyou Cao

Submitted to Journal of the American Chemical Society

December 2016

Condensed Matter Physics and Material Science Department

Brookhaven National Laboratory

U.S. Department of Energy
USDOE Office of Science (SC),
Basic Energy Sciences (BES) (SC-22)

DISCLAIMER

All The Catalytic Active Sites of MoS2 for Hydrogen Evolution

Guoqing Li[1,2], Du Zhang[3], Qiao Qiao[4], Yifei Yu[1], David Peterson[5],, Raj Kumar[1], Stefano Curtarolo[6], Frank Hunte[1], Steve Shannon[5] Yimei Zhu[4], Weitao Yang[3], and Linyou Cao[1,7*]

[1]Department of Materials Science and Engineering, North Carolina State University, Raleigh, NC 27695; [2]College of Textile, North Carolina State University, Raleigh, NC 27695; [3]Department of Chemistry, Duke University, Durham, NC 27708; [4] Department of Condensed Matter Physics and Materials Science, Brookhaven National Laboratory, Upton, NY 11973; [5] Department of Nuclear Engineering, North Carolina State University, Raleigh, NC 27695; [6]Department of Mechanical Engineering and Materials Science, Duke University, Durham, NC 27708; [7]Department of Physics, North Carolina State University, Raleigh, NC 27695.

Abstract

MoS_2 presents a promising low-cost catalyst for the hydrogen evolution reaction (HER), but the understanding about its active sites has been limited. In stark contrast with the common theory, which believes only the edge sites catalytically active, we unambiguously demonstrate that the sulfur vacancies provide another major active site for the HER and that the grain boundaries also show some catalytic activity. The turnover frequencies (Tafel slopes) of the edge sites, sulfur vacancies, and grain boundaries are estimated to be 15 s^{-1} (65-75 mV/dec), 6.3 s^{-1} (65-85 mV/dec), and 0.2 s^{-1} (120-160 mV/dec), respectively. While the catalytic activity linearly depends on the length of edge sites and grain boundaries, it shows a maximum when the density of sulfur vacancies is in the range of 7-10%. The catalytic activity of sulfur vacancies is also related with the crystalline quality at the proximity of the vacancies with higher quality providing higher activity.

* To whom correspondence should be addressed.

Email: lcao2@ncsu.edu

The hydrogen evolution from water stands as an appealing strategy for energy storage. It may store electrical or solar energy in format of chemical fuels (hydrogen) that can be delivered at will and consumed with negligible impact to environment. However, the implementation of this energy storage strategy has been delayed by the imperfection of the catalysts that are required to drive the reaction. Ideal catalysts would feature high catalytic activities and low cost. Noble metals such as Pt can provide excellent catalytic activities for the hydrogen evolution reaction (HER), but are too expensive and scarce to be useful for massive application. Molybdenum disulfide (MoS_2) has been considered to be a promising low-cost alternative.[1-3] This material bears particular implications for the storage of solar energy due to its capability to efficiently absorb solar radiation[4, 5] and fast interfacial charge transfer[6]. Unfortunately, the catalytic activity of MoS_2 is way inferior to that of Pt, and it is necessary to substantially improve the activity for the sake of practical applications.

One key challenge for improving the catalytic activity of MoS_2 is the lack of unambiguous understanding for its catalytically active sites. The common theory believes only the edge sites of MoS_2 to be catalytically active.[7] As a result, the strategies explored to improve the catalytic activity have been overwhelmingly focused on increasing the number of edge sites.[8-14] However, some recent studies have cast serious doubt on the common theory. For instance, MoS_2 with the 1T structural phase is shown exhibiting good catalytic activities, even with substantial oxidation at the edge sites that is expected to destroy the catalytic activity.[15-17] It has also been demonstrated that atomically thin MoS_2 films with little edge sites may be more catalytic active than thick edge-rich pyramid MoS_2 nanoplates.[18, 19] These results strongly suggest that the common theory for the catalytically active site of MoS_2 is far from comprehensive.

Here we have unambiguously demonstrated that, besides the edge sites, the sulfur vacancy of MoS_2 provides another major catalytically active site for the HER. The grain boundary may show some catalytic activity as well. The turnover frequency (TOF) of the edge sites, sulfur vacancies, and grain boundaries are quantitatively evaluated to be $15 \pm 3s^{-1}$, $6.3 \pm 0.8\ s^{-1}$, and around $0.2\ s^{-1}$, respectively. And the typical Tafel slopes are 65-75 mV/dec, 65-85 mV/dec, and 120-160 mV/dec for the edge sites, sulfur vacancies, and grain boundaries. Unlike the linear dependence on the length of the edge sites and grain boundaries, the catalytic activity shows a maximum with the density of sulfur vacancies in the range of 7-10%. Our result indicates that the catalytic activity of the sulfur vacancies is also related with the crystalline quality at the proximity of the vacancies as higher crystalline quality at the proximity may enable higher catalytic activity at the vacancies. The desired structure would be monolayer MoS_2 that involves the optimal density of sulfur vacancies and is otherwise in high crystalline quality. It is worthwhile to point out that a very recent work has also claimed catalytic activities at the sulfur vacancies of MoS_2 for the HER,[20] but the experimental results used to support the claim are misinterpreted and actually cannot support the claim (see S1 of the Supplementary Information). In stark contrast with the previous studies,[20] our experimental results indicate that the sulfur vacancies created by Ar plasma treatment are not catalytically active, which is likely due to an unfavorable crystalline structure at the proximity of the plasma-created vacancies.

We start with examining the catalytic activities of continuous monolayer MoS_2 films and discrete monolayer MoS_2 flakes as shown in Fig. 1a-b. The film and flakes are synthesized on sapphire substrates and then transferred onto glassy carbon substrates for catalytic characterizations using a surface-energy-assisted transfer process that we developed (Fig. 1a-b).[21] More specifically, the film is grown using a self-limiting CVD process previously developed by our group,[22] and the

flakes are synthesized with another CVD process reported in the references.[23] We have previously demonstrated that the crystalline and surface quality of the film and the flakes may be nicely preserved during the transfer process. We have also confirmed that the film is a continuous and highly uniform monolayer with no voids, cracks, and steps (see Ref.22 and Fig. S1). The film is expected to bear little edge sites due to the structural continuity (Fig. 1a). In contrast, the discrete flakes are monolayers in size of 1 micrometer with well-defined edges (Fig. 1b and Fig. S1). The presence of little edge sites at the film is supported by magnetic measurement. It is well known that the edge sites of MoS_2 may provide ferromagnetic moments,[24, 25] and our magnetic measurement indeed shows substantial ferromagnetic moment at the flakes but not at the film (Fig. 1c). According to the common theory,[26] which believes only the edge site catalytically active, one would expect much worse catalytic performance at the film than at the flakes.

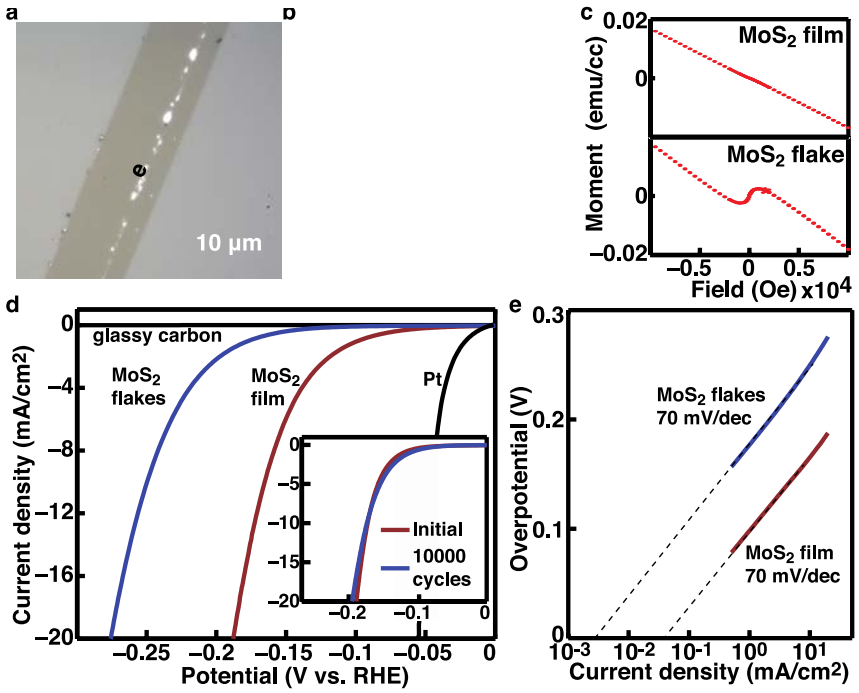

Figure 1. Catalytic activities of continuous monolayer MoS_2 films and discrete monolayer MoS_2 flakes. (a) Optical image of a typical as-grown monolayer MoS_2 film. A scratch is intentionally introduced to show the contrast between the film and the substrate (sapphire). Inset, optical image of a typical film transferred onto a glassy carbon substrate in size of around 1 × 1 cm. (b) Optical image of discrete monolayer MoS_2 flakes. (c) Magnetic measurement results of monolayer MoS_2 films (upper) and flakes (lower). The straight line indicates the diamagnetic moment of the substrate and the curved center represents the ferromagnetic moment of the flakes. (d) Polarization curves of monolayer MoS_2 films (blue) and flakes (red). The polarization curves of glass carbon substrates and Pt are also given as shown. Inset, stability test results of monolayer MoS_2 films. The initial result (red) represents the result collected from the film when its performance appears to be stable after pre-testing cycles (see Methods and Fig. S2). (e) Tafel plots derived from the results given in (d). The dashed lines serve to illustrate the Tafel slope and the exchange current density at 0V overpotential.

In stark contrast with the intuitive expectation, the edge-less monolayer film exhibits much better catalytic activities than the monolayer flakes. Fig. 1d-e shows the polarization curves and corresponding Tafel plots of the film and the flakes. The result for the flakes has already been normalized to the area coverage of the flakes on the substrate. The film can provide a current density of 20 mA/cm^2 at an overpotential of around 0.19 V, which is among the best of what previously reported with all kinds of MoS_2 materials in references.[9-15, 17, 19, 27-31] We can find the Tafel slope and exchange current density by fitting the Tafel plots to the equation of $\eta = \rho\log(j) + \log(j_0)$, where η is the overpotential (vs. RHE), j_0 the exchange current density, and ρ the Tafel slope[32]. Both the film and the flakes show similar Tafel slopes of 70 mV/dec, but the exchange current density of the film is one order of magnitude higher, 40 $\mu A/cm^2$ vs. 3.5 $\mu A/cm^2$ at the flakes. Significantly, the exchange current density of the monolayer film is more than one order of magnitude higher than what previously observed at MoS_2 catalysts.[9-15, 17, 19, 27-31] This is truly remarkable as the MoS_2 materials studied in the previous studies often have surface roughness orders of magnitude greater than our atomically smooth film. Part of the reason for this extraordinarily high exchange current density is rooted in the atomically thin dimension of the monolayer film. We have previously demonstrated that the exchange current density is dependent on the charge transfer efficiency inside MoS_2 and monolayers can best facilitate the charge transfer in the vertical direction.[18] It is worthwhile to note that the monolayer shows remarkable stability with negligible decrease in the catalytic activity even after 10,000 cycles.

We find that the catalytic activity of the flakes can be mainly correlated to the edge sites, which is consistent with the common theory. This is evidenced by a linear dependence of the exchange current density of the flakes on the length of edges as discussed later (see Fig.4d). However, the excellent catalytic activity at the continuous MoS_2 film is unexpected. Previous studies have demonstrated that the catalytic activity of MoS_2 may be substantially improved when its structure is changed from 2H to 1T.[15-17] But we can exclude out the possibility of structural changes to be the reason for the high catalytic activity of the film. We examine the Raman (Fig. 2a) and XPS (Fig. S3) of the monolayers before and after the catalytic reaction, and find no change in the composition and crystalline structure of both the film and flakes. Therefore, the unexpected excellent catalytic performance of the edge-less monolayer film strongly suggests the presence of catalytic active sites other than the edge.

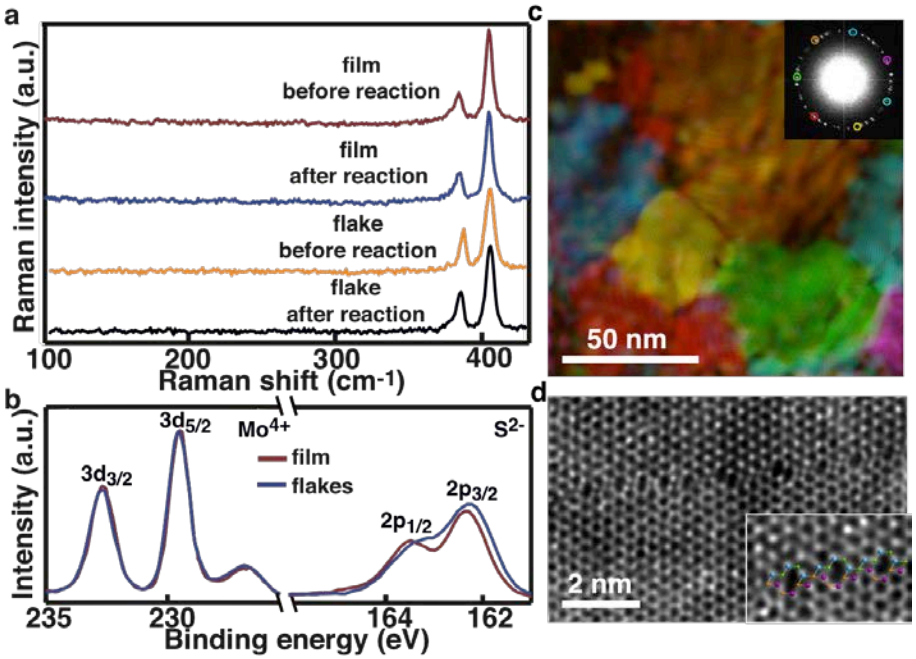

Figure 2. Structural and compositional characterizations of monolayer MoS_2 films and flakes. (a) Raman spectra of monolayer MoS_2 film and flakes before and after the catalytic reaction. The spectra in low wavenumbers are included to indicate no characteristic peaks of 1T MoS_2. (b) XPS results of as-grown MoS_2 film and flakes. c) False color dark field image of the film inverted from the selected spots in the fast fourier transformation (FFT) pattern (shown in the inset) of original high-resolution TEM (HRTEM images. A magnified version of the diffraction pattern is given in Fig. S4. Each area with a different color indicates a grain. (d) STEM annular dark field (ADF) image of a typical grain boundary in the MoS_2 film. Inset shows the 8-4-4 structure at the grain boundary.

To understand the catalytic activity of the film, we examine the possible difference in composition and structure between the film and the flakes. The film is distinguished by the presence of grain boundaries and sulfur vacancies. Unlike the flake, which is well known to be single crystalline, the film is polycrystalline with grain size in the range of 30-100 nm (Fig. 2c-2d). Additionally, XPS measurements show that the stoichiometric ratio of S:Mo in the film is smaller than that of the flakes (Fig. 2b), indicating the presence of sulfur vacancies in the film. However, despite the presence of these crystalline defects, the Raman spectrum of the film is similar to that of the flakes with comparable intensities and lineshapes in the two main characteristic Raman peaks A_{1g} and E^1_{2g} (Fig. S5). This indicates that the film has an overall high crystalline quality but bears some defects including grain boundaries and sulfur vacancies.

Our experimental result indicates that the catalytic activity of the film can be correlated to the sulfur vacancies. We treat the film and the flakes with a process well established to repair sulfur vacancies, and monitor the catalytic activities before and after the repair.[33-35] Briefly, the film and the flake are immersed in (3-mercaptopropyl) trimethoxysilane (MPS) followed by annealing at 300°C. MPS molecules may be adsorbed at sulfur vacancies and transfer sulfur atoms to the vacancies through the dissociation of S-C bonds under elevated temperature as illustrated in Fig.3a. The film shows an obvious decrease in photoluminescence (PL) intensity

and an increase in the S:Mo stoichiometric ratio after the treatment (Fig.3b and Fig. 3c inset), which is consistent with what reported previously and indicates the successful repair of the sulfur vacancies.[35] In contrast, the flakes show negligible change in PL (Fig. 3d inset) and S/Mo ratio (Fig.S6) after the treatment, suggesting the presence of little sulfur vacancies in the flakes as expected. Accordingly, little change can be found in the catalytic performance of the flakes after the repair (Fig. 3d). But the catalytic activity of the film dramatically decreases afterward, the exchange current density decreasing by more than one order of magnitude from 30.1 $\mu A/cm^2$ to 1 $\mu A/cm^2$ and the Tafel slope from 70 mV/dec to 125 mV/dec (see the Tafel plots in Fig. S7). We can exclude out the possible physical covering of residual MPS molecules to be the reason for the decrease in catalytic activity, as it would otherwise give rise to similar decrease in both film and flakes. The negligible physical coating is also supported by AFM measurements that indicate no obvious change in the thickness of the film after the repair treatment (Fig. S8). Therefore, the dramatic decrease in catalytic activity can be ascribed to the elimination of sulfur vacancies by the repair. It indicates that the catalytic activity of the film is mainly contributed by the sulfur vacancies.

Our experimental results also indicate that the catalytic activity of the grain boundaries is weak. This is evidenced by the weak catalytic performance of the film after the repair of sulfur vacancies. With a grain size in the range of 30-100 nm, the film has a considerable amount of grain boundaries. The weak catalytic activity of the grain boundaries is also supported by a poor catalytic performance of the monolayer MoS_2 film with little sulfur vacancies. This vacancy-less film is synthesized with the same process used to grow the flakes and formed by the merge of neighboring flakes in the case of high nucleation densities. We have confirmed that the flake-merged film have identical composition as the individual flakes with little sulfur vacancies by Raman, PL, and XPS measurements. The flake-merged film also has little edge sites due to structural continuity, and its grain size is estimated to be around 1μm. It shows very poor catalytic performance as indicated by the polarization curve given in Fig. 3c (red dashed curve). The exchange current density is as low as 0.04 $\mu A/cm^2$ and the Tafel slope around 160 mV/dec (see the Tafel plot in Fig. S8). We find in experiments that the exchange current density of the repaired and flake-merged films shows a roughly linear dependence on the length of the grain boundaries (Fig. S9). This further supports that the weak catalytic activities of the repaired and the flake-merged films are mainly contributed by the grain boundaries.

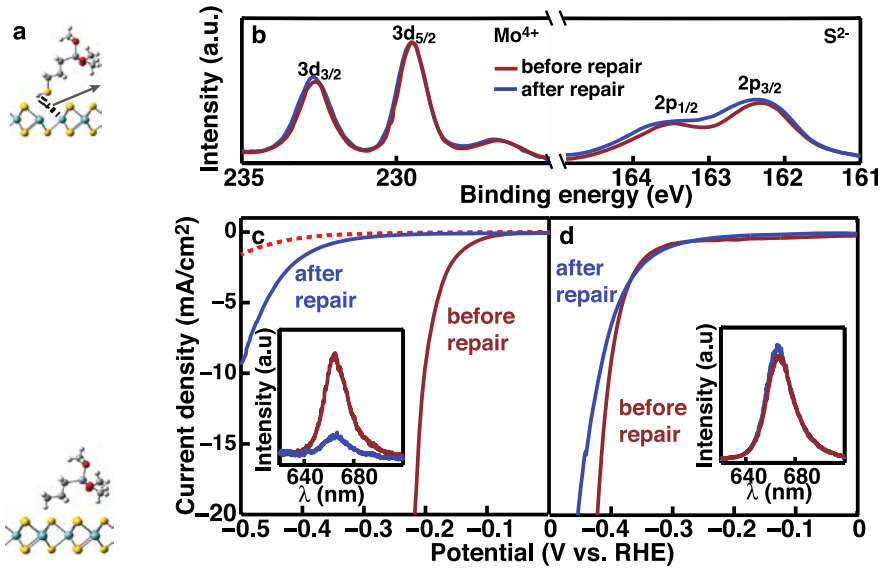

Figure 3. Effect of sulfur vacancy repair on catalytic activity. (a) Schematic illustration for the process of repairing the sulfur vacancies in MoS_2. (b) XPS results of the film before (red) and after (blue) the repair of sulfur vacancies. (b) Polarization curves of the MoS_2 film before (red) and after (blue) the repair of sulfur vacancies. Inset is the PL of the MoS_2 film before (red) and after (blue) the repair. The polarization curve of the flake-merged MoS_2 film with little sulfur vacancies is also given (dashed red). (c) Polarization curves of the MoS_2 flakes before (red) and after (blue) the repair of sulfur vacancies. Inset is the PL of the flakes before (red) and after (blue) the repair.

We can quantitatively evaluate the catalytic activity for each of the different sites, including sulfur vacancies, edge sites, and grain boundaries. In order to evaluate the catalytic activity of single sulfur vacancies, we examine the catalytic performance of monolayer MoS_2 films with different densities of sulfur vacancies. The density of sulfur vacancies is controlled by controlling the growth conditions such as temperature, and may be quantitatively estimated from XPS measurement (Fig. 4a and Fig. S10). We have confirmed that the overall crystalline qualities of all the films are reasonably comparable as indicated by comparable intensities of the characteristic Raman peaks (Fig. S11). Fig. 4b shows the polarization curves collected from these films. The catalytic performance is strongly dependent on the vacancy density. To better illustrate the dependence, we extract the exchange current density and Tafel slope from the measured polarization curves and plot them as a function of the vacancy density in Fig. 4c. The catalytic activity of the film shows a maximum when the density of sulfur vacancies is in the range of 7-10%, with exchange current densities in the range of 30-60 $\mu A/cm^2$ and Tafel slopes in the range of 65-75 meV/dec. We can estimate the turnover frequency (TOF), which indicate the catalytic reaction rate at single active sites, at each sulfur vacancy to be around 6.3 ± 0.8 s^{-1} (the calculation method seen in S2 of the Supplementary Information). As a reference, we also study the catalytic performance of the flakes as a function of the density of edge sites. The result indicates a linear dependence of the exchange current density on the edge length per unit area (Fig. 4d), which is consistent with what reported previously.[11, 26] We can estimate the turnover frequency of each edge site to be around 15 ± 3 s^{-1} (the calculation method seen in S2 of the Supplementary Information). Additionally, we can roughly estimate that the turnover frequency of each grain boundary site is 0.2 s^{-1} from the result given in Fig. S9, more than one or two orders

of magnitude smaller than that of the sulfur vacancies and edge sites. Unlike the exchange current density, the Tafel slope shows much less dependence on the density of catalytic active sites. The Tafel slope usually remains to be in the range of 65-75 mV/dec and 65-85 mV/dec for the edge sites and sulfur vacancies, but may turn to be much larger when the density of the active sites gets to be very small (Fig. 4c-d). The Tafel slope of the grain boundaries is much higher, in the range of 120-160 mV/dec. We do like to point out that the result for the grain boundaries is actually an averaged result over many different types of ground boundaries. In reality, the activity of some grain boundaries could be stronger than others.

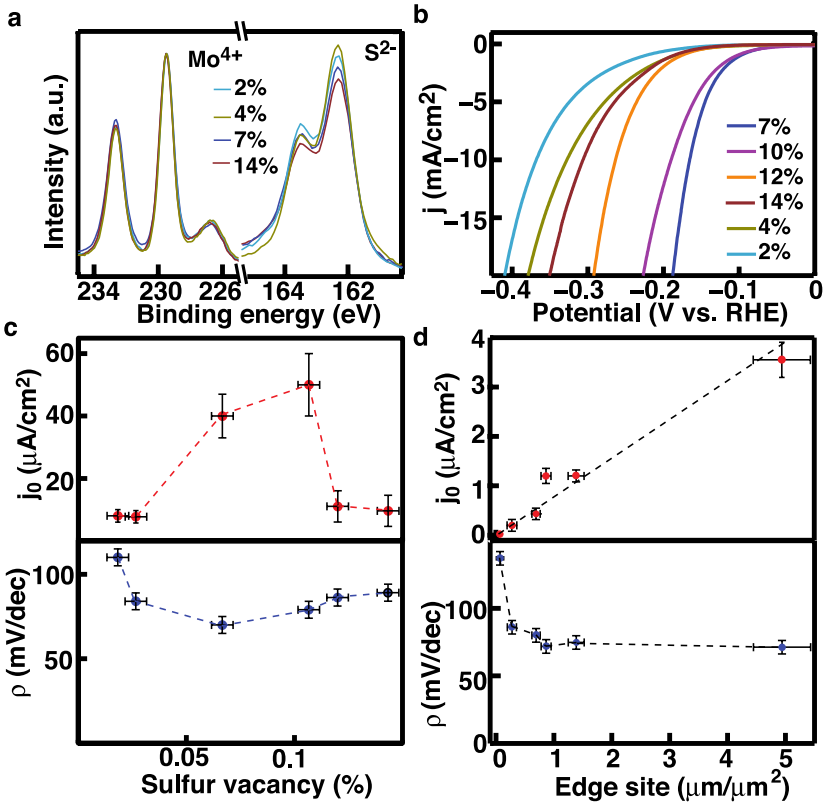

Figure 4. Quantitative evaluation for the catalytic activities of each active site. (a) XPS results for monolayer MoS_2 films with different densities of sulfur vacancies. (b) Polarization curve of the MoS_2 films with different densities of sulfur vacancies. (b) Exchange current densities (upper) and Tafel slopes of the films as a function of the density of sulfur vacancies. The dashed lines serve to guide the vision. (c) Exchange current densities (upper) and Tafel slopes of the MoS_2 flakes as a function of the edge length per unit area. The dashed lines serve to guide the vision.

We can directly visualize the active sites by performing electrochemical deposition of Cu metal (Cu^{2+} ➔Cu^0) at the MoS_2 film and flakes. The treatment of sulfur vacancy repair may substantially suppress the Cu deposition at the film but not at the flakes, similar to the effect of the repair on the HER (Fig. 3c-d). This indicates that the electrochemical deposition of Cu shares the same catalytic active sites with the HER and can be used to directly visualize the catalytic active sites. Fig. 5 shows the Cu particles deposited at the film and the flakes. The Cu particles distribute uniformly everywhere on the MoS_2 film while predominantly at the edge sites for the flakes, which is consistent with our expectation based on the studies of hydrogen

evolution. The Cu deposition may also occur at mirror grain boundaries (Fig. 5c and see the STEM images of mirror and tilt grain boundaries in Fig. S12-S13) but the deposited particles are obviously smaller and less dense than those deposited at the neighboring edge sites. No Cu deposition can be found at tilt grain boundaries (Fig. 5d). This suggests that the mirror grain boundary may have some catalytic activity that is weaker than the edge sites, while the title grain boundary is not catalytically active.

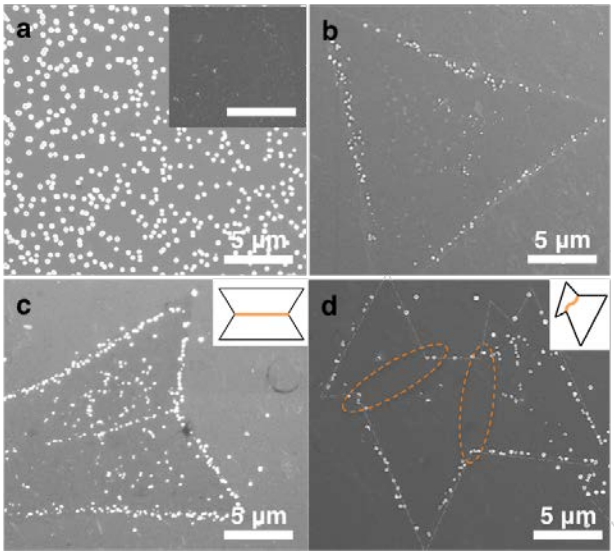

Figure 5. Imaging catalytic active sites with the electrochemical deposition of Cu nanoparticles. (a) SEM images of the Cu particles deposited on MoS_2 films. Inset is the image for the Cu deposition on the MoS_2 film pre-treated with the repair of sulfur vacancies. Scale bar, 10 μm. SEM images of the Cu particles deposited on (b) MoS_2 flakes, (c) MoS_2 flakes with mirror boundaries, and (d) MoS_2 flakes with tilt boundaries. The tilt boundaries are marked with dashed orange ovals. The dashed gray lines in (d) mark the edges of the flake. The insets in (c) and (d) schematically illustrate the mirror and tilt boundaries. More information about the mirror and tilt grain boundaries can be found in Fig. S12 and Fig. S13.

The experimental result is supported by theoretical calculations. We theoretically examine the adsorption free energy of H atoms, which has been widely considered to be a useful indicator for the catalytic activity, at different sites. Generally, an adsorption free energy closer to zero indicates higher catalytic activities.[36] The calculation results are given in Table 1, and they show reasonable consistency with what was observed in experiments. The calculation indeed indicates that the Mo edge and sulfur vacancies are the major catalytically active sites. It also indicates different catalytic activities at various grain boundaries (see grain boundary structures in Fig. S12 and Fig. S13). The 8-4-4 structure, which is involved in the mirror grain boundary, may have some catalytic activity that is weaker than the edge site and sulfur vacancies, and the other types of grain boundaries such as 5-7 structures, which are involved in tilt boundaries, are much less catalytically active.

Table 1. Adsorption free energies of H atoms at different sites.

Sites	ΔG_H^0 (eV)
Mo edge	0.115
S vacancy (1S)	-0.095
Grain boundary (8-4-4)	0.181
Grain boundary (12-4)	0.368
Grain boundary (5-7)	0.566
Basal plane	1.218

As one last note, the catalytic activity of the sulfur vacancies also shows dependence on the local crystalline structure at the proximity of the vacancy. Generally, the monolayer MoS_2 film with low crystalline quality, as indicated by low Raman and PL intensities, exhibits much worse catalytic activity than the counterpart with comparable sulfur vacancies but higher crystalline quality (Fig. S14). With the densities of sulfur vacancies being comparable, the film with lower crystalline quality involves more grain boundaries. The worse catalytic performance suggests that the sulfur vacancies located in or close to grain boundaries are not very active. This observation is consistent with the result of our previous studies. We have previously demonstrated that the monolayer film directly grown on glass carbon substrates, which is in low crystalline quality as indicated by Raman spectra, shows very poor catalytic activity with exchange current density being 1 $\mu A/cm^2$ and Tafel slope of 140 mV/dec.[18] We also find that the sulfur vacancies created by Ar plasma treatment are not catalytic active (see Fig. S15-S17). This likely due to unfavorable crystalline structures at the proximity of the sulfur vacancies as the plasma treatment may likely also introduce other crystalline imperfection like Mo vacancies. We believe that the local environment could affect the electronic structure at the sulfur vacancy and eventually affect the catalytic activity. More studies would be necessary to better understand the effect of the local structure at the proximity of sulfur vacancies on the catalytic performance.

This unambiguous understanding for the catalytically active sites of MoS_2 can provide new insight into the rational design of high-performance MoS_2 HER catalysts. The result indicates that both sulfur vacancies and edge sites may be exploited to improve the catalytic performance of MoS_2, while the grain boundaries may only provide minor benefit. It explicitly suggests that engineering sulfur vacancies provides a better strategy than increasing the number of edge sites, at least from the perspective of viability. According to the TOF of the sulfur vacancies and the edge sites, to achieve catalytic performance comparable to the films with the optimal range of sulfur vacancies (as reported in Fig. 1a) would require a high coverage of well-separated monolayer MoS_2 flakes in size of less than 100 nm, the latter of which is very difficult to obtain in experiments. The result also points out that the desired structure would be MoS_2 films with an overall high crystalline quality but involving an optimal density of sulfur vacancies, as the local crystalline structure at the proximity of the vacancy may strongly affect the activity of the vacancy.

Methods

Synthesis and transfer of monolayer MoS_2 films and flakes: MoS_2 thin films were synthesized using a self-limiting chemical vapor deposition process that we have recently developed.[22] Briefly molybdenum chloride ($MoCl_5$) powder (99.99%, Sigma-Aldrich) was placed at the center of the furnace and sulfur powder (Sigma-Aldrich) at the upstream entry of the furnace. Receiving substrates (sapphire) were placed in the downstream of the tube. Typical conditions include a temperature of 850 °C, a flow rate of 50 sccm, and a pressure around 2 Torr. The film with different densities of sulfur vacancies were grown by varying the growth temperature in the range of 700-900°C. Monolayer MoS_2 flakes were grown using a different chemical vapor deposition (CVD)[6], in which MoO_3 (99.99%, Sigma-Aldrich) instead of $MoCl_5$ was used as the precursor.

The transfer of the monolayers followed a surface-energy-assisted transfer approach that we have developed previously.[21] Briefly, a layer of polystyrene (PS) was spin-coated on the as-grown monolayers. A water droplet was then dropped on the top of the polymer. Due to the different surface energies of the monolayer and the substrate, water molecules could penetrate under the monolayer, resulting the delamination of the PS-monolayer assembly. We could pick up the polymer/monolayer assembly with a tweezers and transferred it to glassy carbon substrates. Finally, PS was removed by rinsing with toluene several times.

Repair of sulfur vacancies: Sulfur repair was conducted following a process reported previously.[33] Basically, monolayer MoS_2 was dipped in a solution of 1/15 (volume ratio) MPS (Sigma-Aldrich)/dichloromethane (Sigma-Aldrich) for 48 hours in a dry glove box. The samples were then rinsed thoroughly with dichloromethane and isopropanol (Sigma-Aldrich), and blown dry with N_2. Finally the samples were annealed in a flow of Ar (with 5% H_2) at 350 °C for 20 minutes.

Structure and Composition Characterizations: Raman measurements were carried out by a Horiba xPlora system equipped with an excitation wavelength at 532 nm. AFM measurements were performed at a Veeco Dimension-3000 atomic force microscope. XPS measurements were carried out at X-ray photoelectron spectroscope (SPECS System with PHOIBOS 150 analyzer using an Mg Kα X-ray source). Annular dark field (ADF) STEM images and HRTEM images were acquired using an aberration corrected JEOL JEM-ARM200CF scanning transmission electron microscope operated at 80kV. ADF images were processed with deconvolution filter to improve contrast. Magnetization measurements were performed at 350 K in a Quantum Design® MPMS SQUID VSM. The magnetic field was applied in the plane of the samples that were mounted on a diamagnetic quartz sample holder.

Electrochemical Characterizations: The electrochemical characterization was performed in 0.5 M H_2SO4 using a CH Instrument electrochemical analyzer (Model CHI604D) with a Pt-wire counter electrode and a saturated calomel reference electrode (SCE). Nitrogen gas was bubbled into the electrolyte throughout the experiment. The potential shift of the SCE is calibrated to be -0.262 V vs. RHE. Typical electrochemical characterizations of the monolayers were performed using linear sweeping from +0 V to -0.5V (vs. RHE) with a scan rate of 5 mV/s. The electrolyte resistance and capacitance of the electrocatalysts were characterized using electrochemical impedance spectroscopy (EIS). The AC impedance is measured within the frequency range of 106 to 1 Hz with perturbation voltage amplitude of 5 mV. An equivalent Randles circuit model

was fit to the data to determine the system resistance and capacitance. The electrochemical deposition of Cu were performed in 1 M $CuSO_4$ by linearly sweeping from +0 V to -0.08V (vs. RHE) with a scan rate of 5 mV/s.

DFT Computation: All computations in this work were performed with the plane-wave software code VASP (Vienne ab initio simulation package)[37]using the Perdew-Burke-Ernzerhof (PBE) exchange-correlation energy functional[38] with its corresponding pseudopotentials. For the H adsorption on the basal plane the Mo edge, 5-7 and 8-4-4 grain boundary sites, the plane wave cutoff was chosen as 480 eV. The Monkhorst-Pack[39] 2×1×1 k-point grid was applied for the geometry optimizations, and the 6×1×1 k-point grid for the single point energy calculations. For the 12-4 grain boundary sites, the plane wave energy cutoff was chosen as 480 eV for the geometry optimizations, and 540 eV for the single point energy calculations. The Monkhorst-Pack 2×1×1 k-point grid was applied for both the geometry optimizations and the single point energy calculations.

Acknowledgements

This work was supported by CCDM, an EFRC funded by U.S. Department of Energy (DOE), Office of Science, Office of Basic Energy Sciences (BES), under award #DE-SC0012575. Y.Z. acknowledges the support by DOE, Office of Science, BES, Materials Sciences and Engineering Division, under contract #DE-SC0012704. The authors acknowledge the use of the Analytical Instrumentation Facility (AIF) at North Carolina State University, which is supported by the State of North Carolina and the National Science Foundation.

Author contributions

G. L. and L.C. conceived the idea, designed the experiments, analyzed the data, and wrote the manuscript. Y.Y. helped with the synthesis and contributed to the data analysis. D. Z., S. C, and W. Y. performed the theoretical calculations and related analysis. Q. Q. and Y. Z. performed the (S)TEM characterization and analysis. R. K. and F. H. performed the magnetic measurements. D. P. and S. S. helped with the Ar plasma treatment. All the people were involved in reviewing the manuscript.

Competing financial interests

The authors declare no competing financial interests.

1. Laursen, A.B., Kegnaes, S., Dahl, S. & Chorkendorff, I. Molybdenum sulfides-efficient and viable materials for electro - and photoelectrocatalytic hydrogen evolution. *Energ Environ Sci* **5**, 5577-5591 (2012).
2. Chhowalla, M. et al. The chemistry of two-dimensional layered transition metal dichalcogenide nanosheets. *Nat Chem* **5**, 263-275 (2013).

3. Merki, D. & Hu, X.L. Recent developments of molybdenum and tungsten sulfides as hydrogen evolution catalysts. *Energ Environ Sci* **4**, 3878-3888 (2011).
4. Huang, L. et al. Atomically Thin Narrowband and Broadband Light Superabsorbers. *Unpublished* (2016).
5. Cao, L.Y. Two-dimensional transition-metal dichalcogenide materials: Toward an age of atomic-scale photonics. *Mrs Bull* **40**, 592-599 (2015).
6. Yu, Y. et al. Equally Efficient Interlayer Exciton Relaxation and Improved Absorption in Epitaxial and Nonepitaxial MoS2/WS2 Heterostructures. *Nano Letters* **15**, 486-491 (2014).
7. Jaramillo, T.F. et al. Identification of Active Edge Sites for Electrochemical H2 Evolution from MoS2 Nanocatalysts. *Science* **317**, 100-102 (2007).
8. Karunadasa, H.I. et al. A Molecular MoS2 Edge Site Mimic for Catalytic Hydrogen Generation. *Science* **335**, 698-702 (2012).
9. Kibsgaard, J., Chen, Z.B., Reinecke, B.N. & Jaramillo, T.F. Engineering the surface structure of MoS2 to preferentially expose active edge sites for electrocatalysis. *Nat Mater* **11**, 963-969 (2012).
10. Kong, D. et al. Synthesis of MoS2 and MoSe2 Films with Vertically Aligned Layers. *Nano Letters* **13**, 1341-1347 (2013).
11. Shi, J.P. et al. Controllable Growth and Transfer of Mono layer MoS2 on Au Foils and Its Potential Application in Hydrogen Evolution Reaction. *Acs Nano* **8**, 10196-10204 (2014).
12. Xie, J. et al. Controllable Disorder Engineering in Oxygen-Incorporated MoS2 Ultrathin Nanosheets for Efficient Hydrogen Evolution. *Journal of the American Chemical Society* **135**, 17881-17888 (2013).
13. Ye, G.L. et al. Defects Engineered Monolayer MoS2 for Improved Hydrogen Evolution Reaction. *Nano Letters* **16**, 1097-1103 (2016).
14. Gao, M.R., Chan, M.K.Y. & Sun, Y.G. Edge-terminated molybdenum disulfide with a 9.4-angstrom interlayer spacing for electrochemical hydrogen production. *Nat Commun* **6** (2015).
15. Voiry, D. et al. Conducting MoS2 Nanosheets as Catalysts for Hydrogen Evolution Reaction. *Nano Letters* **13**, 6222-6227 (2013).
16. Lukowski, M.A. et al. Enhanced Hydrogen Evolution Catalysis from Chemically Exfoliated Metallic MoS2 Nanosheets. *J. Am. Chem. Soc.* **135**, 10274–10277 (2013).
17. Wang, H.T. et al. Electrochemical tuning of vertically aligned MoS2 nanofilms and its application in improving hydrogen evolution reaction. *P Natl Acad Sci USA* **110**, 19701-19706 (2013).

18. Yu, Y. et al. Layer-Dependent Electrocatalysis of MoS2 for Hydrogen Evolution. *Nano Letters* **14**, 553-558 (2014).
19. Tan, Y.W. et al. Monolayer MoS2 Films Supported by 3D Nanoporous Metals for High-Efficiency Electrocatalytic Hydrogen Production. *Advanced Materials* **26**, 8023-+ (2014).
20. Li, H. et al. Activating and optimizing MoS2 basal planes for hydrogen evolution through the formation of strained sulphur vacancies (vol 15, pg 48, 2016). *Nat Mater* **15** (2016).
21. Gurarslan, A. et al. Surface-Energy-Assisted Perfect Transfer of Centimeter-Scale Monolayer and Few-Layer MoS2 Films onto Arbitrary Substrates. *ACS nano* **8**, 11522-11528 (2014).
22. Yu, Y.F. et al. Controlled Scalable Synthesis of Uniform, High-Quality Monolayer and Few-layer MoS2 Films. *Sci Rep-Uk* **3** (2013).
23. Lee, Y.H. et al. Synthesis of Large-Area MoS2 Atomic Layers with Chemical Vapor Deposition. *Advanced Materials* **24**, 2320-2325 (2012).
24. Tongay, S., Varnoosfaderani, S.S., Appleton, B.R., Wu, J.Q. & Hebard, A.F. Magnetic properties of MoS2: Existence of ferromagnetism. *Appl Phys Lett* **101** (2012).
25. Pan, H. & Zhang, Y.W. Tuning the Electronic and Magnetic Properties of MoS2 Nanoribbons by Strain Engineering. *J Phys Chem C* **116**, 11752-11757 (2012).
26. Jaramillo, T.F. et al. Identification of active edge sites for electrochemical H-2 evolution from MoS2 nanocatalysts. *Science* **317**, 100-102 (2007).
27. Benck, J.D., Chen, Z., Kuritzky, L.Y., Forman, A.J. & Jaramillo, T.F. Amorphous Molybdenum Sulfide Catalysts for Electrochemical Hydrogen Evolution: Insights into the Origin of their Catalytic Activity. *ACS Catalysis* **2**, 1916-1923 (2012).
28. Chen, Z.B. et al. Core-shell MoO3-MoS2 Nanowires for Hydrogen Evolution: A Functional Design for Electrocatalytic Materials. *Nano Letters* **11**, 4168-4175 (2011).
29. Li, Y. et al. MoS2 Nanoparticles Grown on Graphene: An Advanced Catalyst for the Hydrogen Evolution Reaction. *Journal of the American Chemical Society* **133**, 7296-7299 (2011).
30. Li, Y. et al. Engineering the Composition and Crystallinity of Molybdenum Sulfide for High-Performance Electrocatalytic Hydrogen Evolution. *ACS Catalysis* **5**, 448-455 (2015).
31. Merki, D., Fierro, S., Vrubel, H. & Hu, X.L. Amorphous molybdenum sulfide films as catalysts for electrochemical hydrogen production in water. *Chem Sci* **2**, 1262-1267 (2011).

32. Bockris, J.O. Pleskov's review of surface electrochemistry: A molecular level approach - Reply. *Russ J Electrochem+* **31**, 1211-1211 (1995).
33. Qiu, H. et al. Hopping transport through defect-induced localized states in molybdenum disulphide. *Nat Commun* **4** (2013).
34. Makarova, M., Okawa, Y. & Aono, M. Selective Adsorption of Thiol Molecules at Sulfur Vacancies on MoS2(0001), Followed by Vacancy Repair via S-C Dissociation. *J Phys Chem C* **116**, 22411-22416 (2012).
35. Cho, K. et al. Electrical and Optical Characterization of MoS2 with Sulfur Vacancy Passivation by Treatment with Alkanethiol Molecules. *Acs Nano* **9**, 8044-8053 (2015).
36. Hinnemann, B. et al. Biornimetic hydrogen evolution: MoS2 nanoparticles as catalyst for hydrogen evolution. *Journal of the American Chemical Society* **127**, 5308-5309 (2005).
37. Kresse, G. & Furthmuller, J. Efficient iterative schemes for ab initio total-energy calculations using a plane-wave basis set. *Phys Rev B* **54**, 11169-11186 (1996).
38. Perdew, J.P., Burke, K. & Ernzerhof, M. Generalized gradient approximation made simple. *Phys Rev Lett* **77**, 3865-3868 (1996).
39. Monkhorst, H.J. & Pack, J.D. Special Points for Brillouin-Zone Integrations. *Phys Rev B* **13**, 5188-5192 (1976).